



Effects of Chemical Alteration on Frictional Properties in a Deep, Granitic, Geothermal System in Cornwall: Direct Shear Experiments at Near In Situ Conditions

N. Harpers^{1,2} , N. Forbes Inskip¹, M. J. Allen³ , J. Buckman¹, D. R. Faulkner³ , H. Claes⁴, R. Shail⁵ , S. den Hartog^{1,6} , and A. Busch¹

¹Heriot-Watt University, The Lyell Centre, Edinburgh, UK, ²RWTH Aachen University, Applied Structural Geology Teaching and Research Unit, Aachen, Germany, ³University of Liverpool, Liverpool, UK, ⁴Department of Earth and Environmental Sciences, Geology, KU Leuven, Leuven, Belgium, ⁵University of Exeter, Camborne School of Mines, Penryn, UK, ⁶Now at State Supervision of Mines, Ministry of Economic Affairs and Climate Policy, The Hague, The Netherlands

Key Points:

- Large fault systems are targeted at depth as geothermal reservoirs in high-heat producing granites in Cornwall
- Direct shear experiments were conducted on a series of successively more naturally altered granites from a fault in Carnmenellis granite
- Alteration makes sliding more likely but also more stable, while higher temperatures destabilize shearing

Supporting Information:

Supporting Information may be found in the online version of this article.

Correspondence to:

N. Harpers,
n.harpers@asg.rwth-aachen.de

Citation:

Harpers, N., Forbes Inskip, N., Allen, M. J., Buckman, J., Faulkner, D. R., Claes, H., et al. (2024). Effects of chemical alteration on frictional properties in a deep, granitic, geothermal system in Cornwall: Direct shear experiments at near in situ conditions. *Journal of Geophysical Research: Solid Earth*, 129, e2024JB028861. <https://doi.org/10.1029/2024JB028861>

Received 31 JAN 2024

Accepted 11 OCT 2024

Author Contributions:

Conceptualization: N. Harpers, N. Forbes Inskip, D. R. Faulkner, R. Shail, S. den Hartog, A. Busch

Data curation: N. Harpers, N. Forbes Inskip, M. J. Allen, J. Buckman

Formal analysis: N. Harpers, N. Forbes Inskip, M. J. Allen, J. Buckman,

D. R. Faulkner, H. Claes, S. den Hartog

Investigation: N. Harpers, M. J. Allen, J. Buckman

Methodology: N. Harpers, N. Forbes Inskip, M. J. Allen, D. R. Faulkner,

H. Claes, R. Shail, S. den Hartog, A. Busch

Resources: J. Buckman, D. R. Faulkner, H. Claes

Abstract The geochemical alteration of host rocks might affect the productivity and the potential for induced seismicity of geothermal systems. In addition to natural alteration, following production and heat extraction, re-injected fluids at lower temperatures and different pressures may be in chemical disequilibrium with the rock, impacting mineral solubility and dissolution/precipitation processes. In this study, we investigate the effect of geochemical alteration on the frictional behavior of granites, and their seismogenic potential, by conducting direct shear experiments using samples with varying degrees of alteration. The samples originate from the Carnmenellis granite in Cornwall, SW England, and represent the formation used in the United Downs Deep Geothermal Power Project for heat extraction. Experiments were conducted on granite powders (referred to as gouges) at room temperature and 180°C, at simulated in situ confining and pore pressures of 130 and 50 MPa, respectively (~5 km depth). With increasing degree of alteration, the frictional strength of the gouges decreases while frictional stability increases. At high temperature, frictional stability is reduced for all samples while maintaining the trend with alteration stage. Microstructural investigation of the sheared gouges shows alteration delocalizes shear by reducing grain size and increasing clay fraction, which promotes the formation of pervasive shear fabrics. Our work suggests that, within the range of tested pressures, more alteration of granite initially causes more stable shearing in a fault. This behavior with alteration is sustained at high temperatures, but the overall frictional stability is reduced which increases the potential for induced seismicity at higher temperatures.

Plain Language Summary Geothermal systems are of high interest as renewable energy source. However, hot fluids in the deep subsurface can chemically react with the host rock they flow through. These reactions then affect the fluid chemistry and the rock mineral composition. With changes in mineral composition, changes in mechanical and hydraulic properties are observed. We test the effects of a specific group of reactions (argillic alteration) on the frictional properties of granite powders by using an example rock that is targeted in geothermal projects in Cornwall, SW England. The frictional properties give information about how likely it is for granitic rocks to produce an earthquake while sliding. Our tests show that the more the granite has chemically changed, the easier the powder is to slide but the more stably it will slide. This means that chemically changed powders are less likely to create seismic waves on sliding. In addition, tests at high temperature (180°C) showed the same stabilizing effect within the reacted rocks but the general sliding stability was reduced over all samples. This implies that the potential for earthquakes is higher at higher temperatures, although the analyzed chemical reactions reduce this potential in granitic geothermal systems.

1. Introduction

Transitioning toward renewable and carbon neutral energy generation is one of the major tasks during the 21st century. In addition to wind or solar energy, harnessing the Earth's geothermal heat can help diversify national green energy portfolios, particularly as geothermal energy projects can deliver a continuous supply of heat and/or power. In the United Kingdom, one of the most promising areas for deep geothermal energy production is Cornwall, SW England (Busby & Terrington, 2017). This region is underlain by the Cornubian batholith, with several large granitic plutons now revealed by erosion. Granites often contain higher concentrations of uranium,

© 2024. The Author(s).

This is an open access article under the terms of the [Creative Commons Attribution License](https://creativecommons.org/licenses/by/4.0/), which permits use,

distribution and reproduction in any medium, provided the original work is properly cited.

Supervision: N. Forbes Inskip, J. Buckman, D. R. Faulkner, S. den Hartog, A. Busch
Visualization: N. Harpers, J. Buckman
Writing – original draft: N. Harpers, N. Forbes Inskip, S. den Hartog, A. Busch
Writing – review & editing: N. Harpers, N. Forbes Inskip, M. J. Allen, J. Buckman, D. R. Faulkner, H. Claes, R. Shail, S. den Hartog, A. Busch

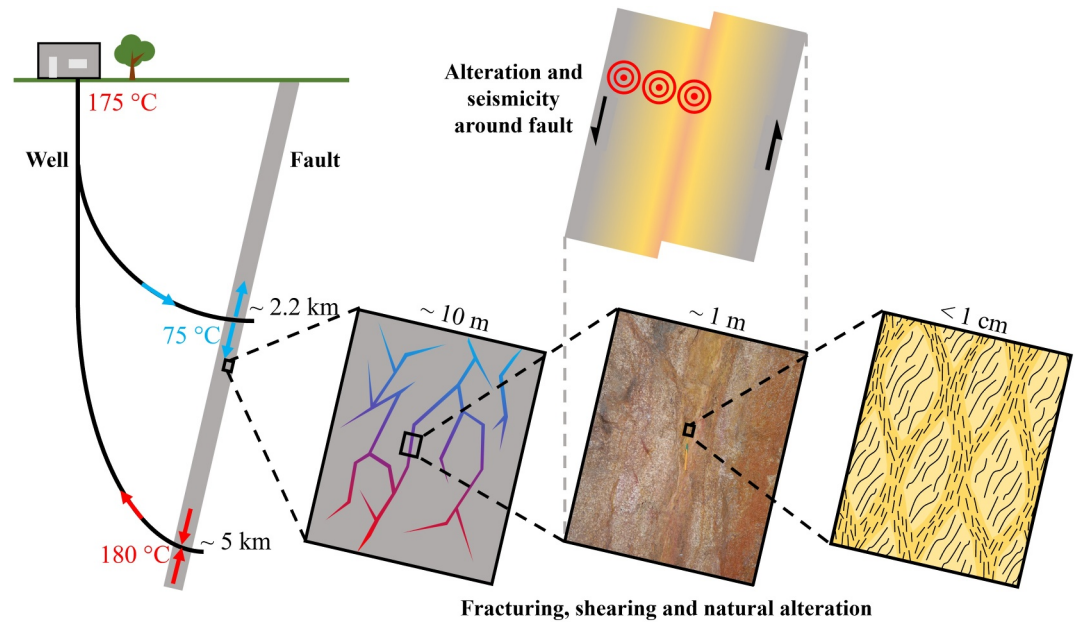


Figure 1. (left) Schematic of the UDDGP project; Porthtowan fault zone as reservoir for fluid production and reinjection. (right) Rock undergoes temperature and pressure changes under geothermal operation. This potentially geochemically alters the rock along the flow paths changing the mineralogy around the fault. New mineralogy causes the formation of other shear structures and changes frictional properties that affect the potential of induced seismicity (modified after Ledingham et al., 2019).

thorium and potassium relative to their host rocks (Abesser et al., 2020). The decay of these elements causes enhanced heat flow which, in the case of Cornwall, is close to double the UK average (Busby & Terrington, 2017). This makes the region a target for geothermal operations like the United Downs Deep Geothermal Power project (UDDGP; see Figures 1 and 2) in the Carnmenellis pluton or the Eden Project in the St. Austell pluton

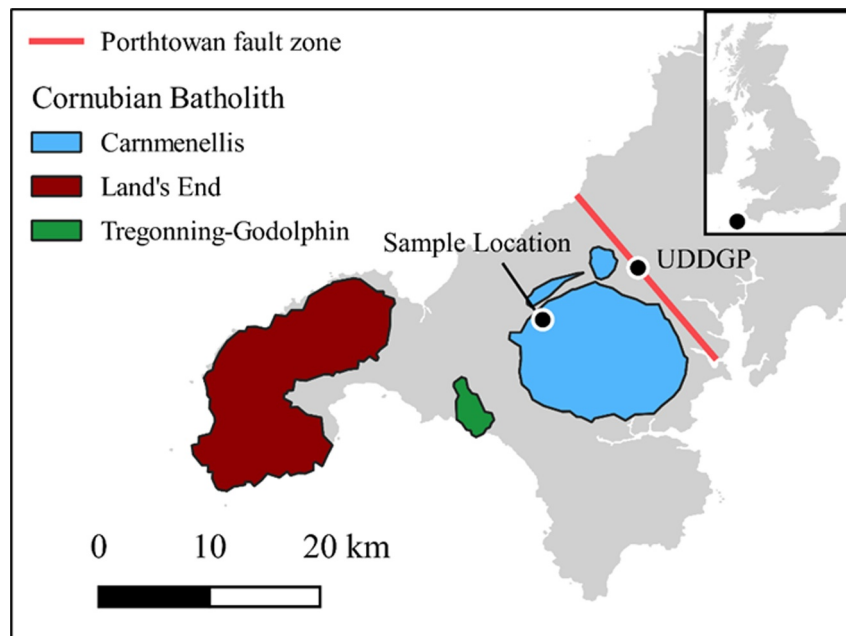


Figure 2. Map of south-west Cornwall indicating the locations of three major plutons. The plutons are part of the Cornubian Batholith emplaced during early Permian post-collisional extension. Sampling location (Holman's Test Mine) is shown and the approximate position and strike of the Porthtowan fault zone (modified after Simons et al., 2016).

(Ledingham et al., 2019, and edengeothermal.com, 2022). These projects target fractures and fault zones in crystalline rock that provide pre-existing pathways for the production of hot fluids (~180°C) and then the re-injection of cooler fluids following heat extraction (e.g., Ledingham et al., 2019).

The sustainability and reliability of these systems depends on the stability of the fault transport properties throughout the lifetime of the system. After heat is extracted, fluids are re-injected into the subsurface at temperatures and pressures that may not be in equilibrium with the surrounding rock. Consequently, the fluids may not be in chemical equilibrium with the surrounding rock, which may promote geochemical reactions to occur (e.g., Kamila et al., 2021; Stefansson, 1997). Mechanical and/or geochemical rock property changes occurring over extended periods of time (i.e., years), can impact the productivity of the system (e.g., Bischoff et al., 2024; Forbes Inskip et al., 2023). Furthermore, given that fault frictional properties depend on mineralogical composition (e.g., Fang et al., 2018; Ikari et al., 2011; Summers & Byerlee, 1977; Tembe et al., 2010), this might impact the risk for induced seismicity (Scholz, 1998).

The frictional properties of granite are relatively well understood over a wide range of conditions (e.g., Biegel et al., 1992; Blanpied et al., 1995; Byerlee, 1967; Hadizadeh et al., 2015; Ishibashi et al., 2018; Mitchell et al., 2016; Wang & Scholz, 1994). However, in most previous studies unaltered granite was used. At room temperature, unaltered granite gouges were found to exhibit stable sliding under a wide range of conditions. These only transition into potentially unstable sliding at high sliding velocities under high effective pressures (Kilgore et al., 1993) or at displacements of 10–100 mm in high displacement tests (Beeler et al., 1996). Blanpied et al. (1998) found that unaltered granite gouges transition from stable sliding to potentially unstable sliding between 90°C and 350°C at 400 MPa effective pressure and 100 MPa pore pressure. This temperature window is relevant to the UDDGP project which operates between ~180°C at the production well and ~80°C at the injection well based on projected temperature gradients (Busby & Terrington, 2017; Ledingham et al., 2019), but also applies to other geothermal systems which work at similar temperature ranges.

Natural fault systems, however, often show geochemical alteration, usually becoming more distinctive with increasing proximity to the fault core (e.g., Nishimoto & Yoshida, 2010). Studies that have considered granite alteration have focused on the alteration mechanisms (e.g., Bartier et al., 2008; Nishimoto & Yoshida, 2010; Savage et al., 1987) or other rock mechanical properties (e.g., Chen et al., 2018; Coggan et al., 2013) instead of friction. Meller and Kohl (2014) considered both chemical alteration and rock frictional behavior and analyzed the impact of hydrothermal alteration zones on the mechanical behavior in granite at Soultz-sous-Forêts (France). They compared borehole logs and friction literature for different rock types and clast clay mixtures and related alteration state and bulk clay content of the rock to frictional strength. Furthermore, they observed on the geothermal reservoir scale that large seismic events were limited to unaltered granite, while clay-rich zones only hosted small magnitude events. However, Meller and Kohl (2014) only related this to friction coefficients from the literature and neglected frictional stability (defined here in terms of the rate and state friction parameters ($a-b$), as described in the data processing section later) as important factor for nucleation of seismic events.

Trends in frictional behavior have been linked to microstructural changes, for mono-mineral powders (e.g., Bedford & Faulkner, 2021; Beynon & Faulkner, 2020; Leclère et al., 2016), and synthetic multi-mineral powder mixtures (e.g., Bedford et al., 2022; Bos et al., 2000; Tembe et al., 2010). While this research provides important fundamental insights, natural rocks often contain more than three minerals and the minerals mechanically interact during shearing, creating complex microstructures. To investigate the links between friction and microstructure in nature, ground-up complex rocks were tested (e.g., He et al., 2007; Hunfeld et al., 2017; Okuda et al., 2023), including granite (e.g., Beeler et al., 1996; Hadizadeh et al., 2015; Ikari et al., 2011). Although, granite friction was analyzed at hydrothermal conditions (e.g., Blanpied et al., 1995) and with respect to geothermal systems (e.g., Zhang et al., 2023), nobody has yet linked their microstructural observations to friction and seismicity in geothermal systems or to the effects of natural geochemical alteration on friction.

In this study, we investigate the effect of geochemical alterations on the frictional behavior and microstructure in granitic fault systems (Figure 1). The key questions addressed here are: Does natural alteration promote or inhibit unstable sliding and with this induced seismicity? How is the friction behavior related to structural changes triggered by alteration? We conducted a series of direct shear experiments at room temperature (18°C) and at 180°C under near in situ stress conditions on Cornish granites, representative of the fault zone targeted in the UDDGP project. We prepared gouges from a sequence of samples from the fault zone with increasing proximity

to the fault core exhibiting different stages of natural chemical alteration. Following the shear-experiments, we prepared thin sections from the deformed gouges and analyzed the development of the gouge microstructure.

2. Materials and Methods

2.1. Sample Material

We collected granite samples from the Carnmenellis pluton in SW Cornwall, England. The pluton is part of the Cornubian batholith that spans from the Isles of Scilly in the SW to the Dartmoor pluton in the NE (Bott et al., 1958). The batholith was emplaced during Early Permian post-collisional extension and the Carnmenellis pluton was dated to be 293.7 ± 0.6 Ma (Chesley et al., 1993). The pluton contains significant amounts of biotite and muscovite, is medium- to coarse-grained and contains potassium feldspar phenocrysts (<25 mm) that make up <5 to 25 wt-% of the rock (Simons et al., 2016).

The granite samples analyzed have been collected in Holman's Test Mine which is located about 1.5 km SE of Camborne (Figure 2, exact coordinates of entrance: $50^{\circ}11'02.0''N$ $5^{\circ}17'00.3''W$) and comprises over 2 km of tunnels and galleries arranged in a grid layout, at depths up to 30 m below surface, in the Carnmenellis pluton. It was selected for sampling because rocks from the mine are less weathered than surface outcrops and there is good 3D exposure of faults within the granite. The granite at the mine hosts two sets of low-displacement (<5 m) faults: (a) ENE-WSW striking, moderately to steeply inclined, extensional faults that are associated with variably developed quartz-tourmaline-chlorite-fluorite-sulfide magmatic-hydrothermal mineralization (Early to Mid Permian in age), (Shail & Simons, 2023), and (b) NW-SE to N-S striking, steeply inclined, faults that typically bring about a small (<5 m) dextral separation of (a) and are associated with chalcidony/quartz \pm hematite veins and wallrock argillic and hematite alteration due to the migration of lower temperature basinal brines (Shail & Simons, 2023).

These relations result in the later faults being termed “cross-courses.” Some cross-courses may have initiated as transfer faults during the development of extensional magmatic-hydrothermal fault systems. However, the principal episodes of cross-course fault development and associated fluid flow was in the Late Permian to Triassic due to ENE-WSW extension during rifting across southern England (Scrivener et al., 1994; Chadwick & Evans, 1995; Shail & Alexander, 1997); this was followed by selective reactivation as strike-slip faults during Cenozoic intraplate shortening (Dearman, 1963). Larger trace-length versions of these faults, with displacements >100 m, have been targeted in the UDDGP (Porthtowan fault zone) and Eden (Great cross-course) projects, and also exhibit evidence for argillic and hematitic alteration, (e.g., Reinecker et al., 2021). We therefore consider the small-displacement cross-courses at Holman's Test Mine to be a suitable analog for our study, and relevant for geothermal energy projects in Cornwall.

We here study the alteration across two low (<5 m) displacement faults in Holman's Test Mine as an analog for alteration in the Porthtowan fault zone at depth. The samples were collected at variable distances to the fault core (Figure 3) to capture increasing granite alteration with decreasing distance to the fault core, which was confirmed by XRD mineralogical analysis (Table 1). With increasing proximity to the fault core (see Figure 3), the samples show increasing clay (up to 25 wt-%) and decreasing plagioclase (down to 0 wt-%). The sample from within the fault core (TM8) shows the highest quartz (59 wt-%) and a slightly lower clay content (22 wt-%). Smectite + chlorite contents increase (2%–11%) closer to the fault core while muscovite + biotite + illite contents decrease (18%–10%), indicating progressive alteration toward the fault core. Sample Sa6 was collected from another cross-course fault from the same mine for comparison purposes. The fault strikes parallel to the main fault sampled but was located approximately 50 m further east in a parallel drive. Sa6 contains higher amounts of kaolinite and lower amounts of smectite + chlorite compared to TM samples. Sa6 indicates the potential variability in the composition of rock that underwent argillic alteration, while the overall mechanism of decreasing plagioclase and increasing clay content is the same.

Sample preparation involved crushing the samples mechanically to cm-sized pieces. Samples were then milled in an agate disc mill for 30–90 s. The powders obtained were subsequently sieved to <125 μm to ensure a uniform maximum grain size. Milling and sieving was repeated until all material passed through the sieve to avoid fractionation. This sample powder represents fault gouge to study friction behavior.

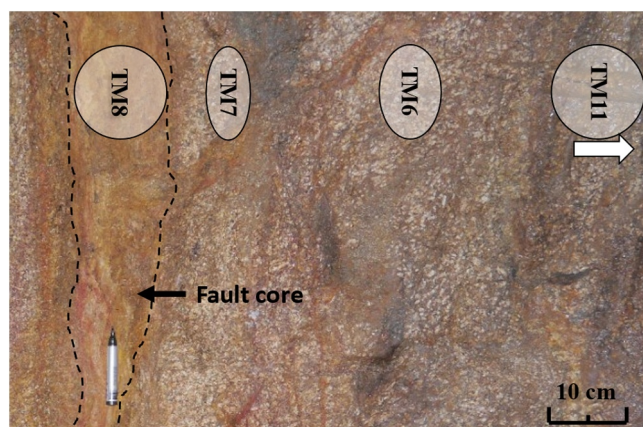


Figure 3. Image of a cross-course structure in Holman's Test Mine with markers of approximate sampling locations. The position of the fault core is marked by dashed lines and the marker was placed for scale. The width of the tags represents the approximate volume from where each sample was taken. TM11 was collected one meter away and is considered unaltered. Sa6 was collected from another cross-course structure in the mine (Table 1).

sample-spacer set is wrapped in a thin sheet of Polytetrafluorethylene (PTFE) to reduce friction between sliders and the surrounding jacket. The jacket consists of Polyvinyl chloride (PVC) in low temperature experiments and of Viton rubber in high temperature experiments. A thin PTFE disk was fitted to the top of the jacketed sliders to allow for small lateral displacements of the sliders during pressurization and compaction of the gouge layer. A detailed description and a schematic of the direct shear assembly are provided in Faulkner et al. (2018).

2.3. Experimental Procedure

Most shear experiments were performed at a confining pressure P_c of 130 MPa and a pore fluid pressure P_p of 50 MPa, leading to an effective pressure $P_{eff} (=P_c - P_p)$ of 80 MPa on the sample. These pressures correspond

2.2. Triaxial Apparatus and Direct Shear Assembly

Our experiments were performed using a triaxial deformation apparatus at the University of Liverpool. The apparatus allows the application of confining pressures of up to 250 MPa and pore pressures up to 200 MPa using two servo-controlled fluid systems. The axial piston moves via a servo-controlled gear train and can be operated by a force or displacement feedback loop. An internal force gauge measures differential axial load of up to 300 kN. Three external furnaces control experimental temperatures while the axial force gauge at the bottom of the vessel is water-cooled to reduce thermal drift. The apparatus is described in detail in Faulkner and Armitage (2013).

The direct shear assembly used in our experiments consists of two L-shaped sliders, between which a 20×36 mm gouge slab is located (Figure 4). Pore pressure reaches the sample through porous stainless-steel frits that are push fitted into the slider surfaces. 1.3 g of dry sample powder were evenly distributed on one of the sliders. We then pre-compressed the powder onto the sliders at about 5 MPa stress normal to the slider surface to create a gouge layer of ~ 1 mm thickness. To ensure coupling between gouge and slider, the contact surface of the slider is made up of a series of 100 μ m deep machined grooves. Silicone rubber spacers accommodate the displacement via elastic compression and stabilize the assembly. The combined slider-

to the lithostatic and hydrostatic pressures in a granite body at 5 km depth, respectively, and were chosen to be comparable to the conditions at the bottom of the production well at UDDGP (Paulillo et al., 2020). We used room temperature experiments to initially investigate the effect of gouge composition and then tested at 180°C to analyze temperature effects. The axial piston was advanced at fixed rates, compressing the slider setup, and causing shear deformation of the samples. Following a run-in phase of 0.3 μ m/s for 1.5 mm, the axial displacement rate was stepped every 0.5 mm between 0.3, 1, and 3 μ m/s until a maximum displacement of 5 mm was reached (velocity sequence displayed in detail in Figure 5). A slow run-in velocity was chosen to ensure the shear-enhanced compaction of the gouge did not result in pore-fluid pressure transients within the gouge layer that might affect mechanical results (Faulkner et al., 2018). Load point displacement (resolution $\pm \sim 0.5$ μ m), confining pressure (± 0.01 MPa), pore fluid pressure (± 0.01 MPa), axial load (± 0.05 kN), and temperature (± 0.1 °C) were measured, and the corresponding signals logged at a frequency of 10 Hz. We conducted more than the experiments that are subject of this paper, but due to the high pressures and partially very high temperatures, experiments have been challenging to conduct. Unfortunately, pump failures and leaks occurred frequently. Data of tests with leaks show reproducibility up to the point when the leak occurred. Examples for such data together with a list of all conducted experiments are shown in Supporting Information S1.

Table 1

XRD Results for Granitic Samples Used in This Study in wt-%

Mineral	Sa6	TM8	TM7	TM6	TM11
Quartz	37	59	31	31	31
Plagioclase	1	0	2	8	20
K-Feldspar	38	18	37	36	28
Ankerite	<0.5	<0.5	<0.5	<0.5	0
Anhydrite	<0.5	<1	1.5	<0.5	0
Tourmaline	<1	<0.5	<0.5	<1	<1
Total clay	20	22	25	23	21
Msc + Bio + Ill ^a	10	10	13	12	18
Kaolinite	7	1	2	2	1
Chl + Sme ^b	3	11	11	9	2
Unknown ^c	3	0	3	2	<1

Note. TM8 to TM11 are ordered by decreasing proximity to fault core, with TM8 having been collected within the core. Sa6 was collected at another fault for comparison. Error for non-clays <1%; Error for clays 1%–2%, but direct comparison of samples allows correct estimate of relative clay contents between samples. ^aMuscovite, Biotite, and Illite. ^bChlorite and Smectite. ^cAmorphous and not identifiable components.

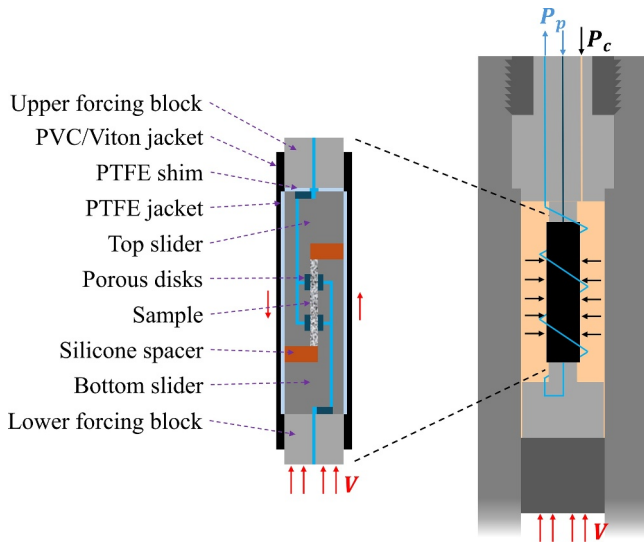


Figure 4. Schematic drawing of the triaxial rig and a detailed view of the direct shear assembly (modified after Faulkner et al., 2018).

Following the experiments, the sheared gouge slabs were carefully taken out of the assembly and left to dry at room temperature for several days. They were then impregnated with epoxy resin to conserve structure and stabilize the thin slab for thin section preparation. Thin sections were cut perpendicular to the shear surface and tangential to the shear direction. We polished the section and analyzed them using Scanning-Electron Microscopy (SEM) as well as Energy-Dispersive X-ray Spectroscopy mapping (EDS mapping) using a Quanta 650 FEG SEM.

We used Avizo, a software application for data visualization by Thermo-Fisher Scientific, to analyze and quantify trends in the microstructure by processing the SEM images of the thin sections. The images were denoised using a non-local means filter and the gray levels readjusted using sigmoidal intensity remapping. We then segmented the images through thresholding and analyzed the segmented particles for grain size (as grain area a_i), grain shape (as aspect ratio of a fitted ellipsoid AR_i), and grain orientation. The latter is calculated as the angle between the gouge layer and the direction of the maximum Feret diameter of a grain in the 2D image. The Feret diameter of a grain at a specific angle describes the distance between two parallel lines perpendicular to that angle enclosing a grain at its outside boundary. It is comparable to the diameter that would be measured with a caliper, if the caliper was fixed to the image plane with the ruled scale of the caliper positioned parallel to the specific angle of interest. Furthermore, we filtered out all grains smaller than 8 pixels because they are close to the image resolution, limiting interpretation of shape and orientation. This filtering of the smallest grain portion and everything below will be addressed in the discussion section.

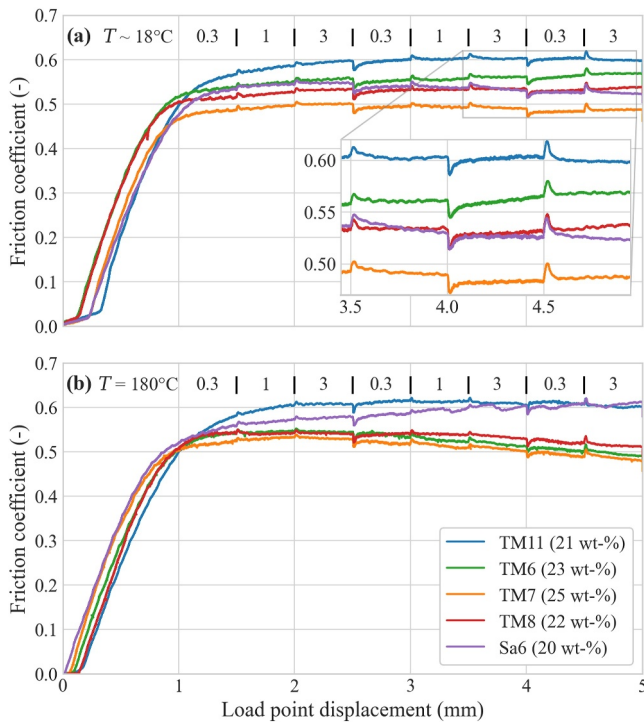


Figure 5. Friction coefficient against load point displacement for all samples tested, at room temperature $\sim 18^\circ\text{C}$ (top) and at 180°C (bottom), $P_{\text{eff}} = 80 \text{ MPa}$. Velocity steps are in $\mu\text{m/s}$ and are marked on top of the graphs. Percentages in the legend indicate the clay content in the sample.

2.4. Data Processing

The axial load applied during each experiment was converted into shear stress τ on the gouge sample which we used to calculate the apparent coefficient of friction according to $\mu = \tau/\sigma_{\text{eff}}$. Effective normal stress σ_{eff} is the difference between normal stress σ , which in our setup is induced by the confining pressure, and pore fluid pressure P_p , that is, $\sigma_{\text{eff}} = \sigma - P_p$. Following Behnen and Faulkner (2012), cohesion and jacket strength are ignored. The data were analyzed using the Rate-and-State Friction (RSF) framework (Dieterich, 1978, 1979; Ruina, 1983) to interpret the velocity dependence of the friction coefficient according to:

$$\mu = \mu_0 + a \ln\left(\frac{V}{V_0}\right) + b \ln\left(\frac{V_0 \theta}{D_{\text{RS}}}\right) \quad (1)$$

here, θ is a gouge state variable, a determines the magnitude of the instantaneous change in μ upon a given step change in sliding velocity from a reference value V_0 to a new value $V = eV_0$, b reflects the magnitude of the change in μ during the evolution to a new steady state value over a critical sliding distance D_{RS} , and μ_0 is the steady state friction coefficient measured at the reference velocity V_0 . For the state variable θ we used Dieterich's aging law formulation (Dieterich, 1979):

$$\dot{\theta} = 1 - \frac{V\theta}{D_{\text{RS}}} \quad (2)$$

For changes in the steady state friction coefficient μ_{ss} resulting from a step-wise change in sliding velocity Equations 7 and 8 yield (e.g., Marone, 1998):

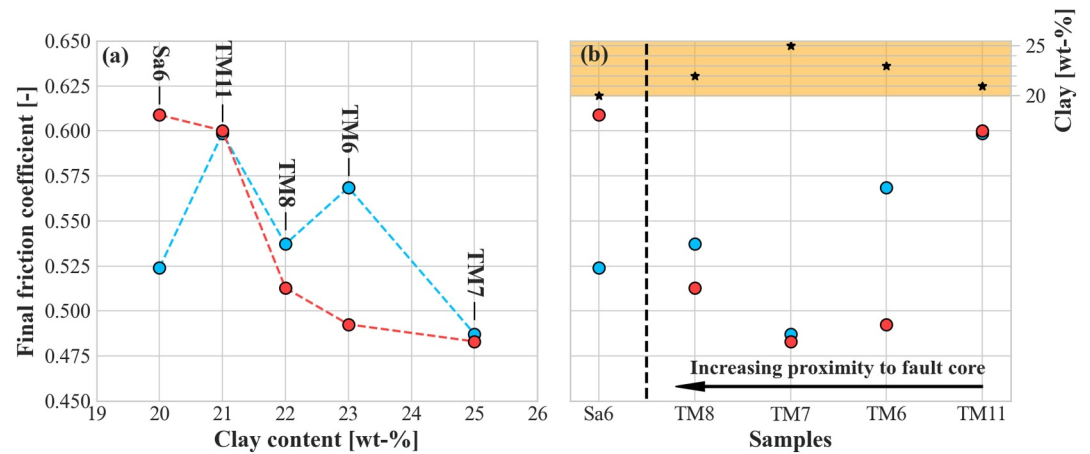


Figure 6. Final friction coefficient calculated as mean over the last 0.4 mm displacement versus (a) clay content and (b) relative position in the fault. In (b) Samples are ordered by increasing proximity to fault core while Sa6 was collected at another fault and used as a reference here. Blue dots indicate room temperature results ($\sim 18^{\circ}\text{C}$); red dots represent high temperature results (180°C).

$$\frac{d\mu_{ss}}{d(\ln V)} = (a - b) \quad (3)$$

A positive $(a - b)$ value indicates that the friction coefficient increases with higher velocities while a negative value of $(a - b)$ indicates a decrease in friction coefficient with an increase in velocity. Systems that exhibit positive $(a - b)$ values are therefore called “velocity-strengthening” (VS) and slip in such systems is intrinsically stable. In contrast, systems that show negative $(a - b)$ values are called “velocity-weakening” (VW) and have the potential to nucleate unstable slip (e.g., Scholz, 2019). We used the MATLAB software package RSFit3000 by Skarbek and Savage (2019) to obtain the Rate-and-State Friction parameters. The software uses a nonlinear least-squares fitting routine for fitting a RSF model to a velocity step and outputs the related parameters.

3. Results

3.1. Direct Shear Experiments

Figure 5a shows representative curves of friction coefficient μ versus load point displacement for all samples at room temperature ($\sim 18^{\circ}\text{C}$) and 80 MPa effective pressure. From displacements of 0.1 mm to 0.9–1.2 mm, μ increases steeply and quasi-linearly to values of 0.43–0.52, when the apparent yield point is reached. Following yielding, the friction coefficients of the gouges generally continue to gently increase with displacement until a displacement of 2 mm. Thereafter, the samples continue to show similar behavior as all reach a steady state before the final displacement of 5 mm. However, their final friction coefficients are different with TM11 reaching the highest value of ~ 0.6 and TM7 the lowest value of ~ 0.49 .

Figure 5b shows friction coefficient μ versus load point displacement for the experiments performed at 180°C . Similar to measurements performed at 18°C , μ increases steeply and quasi-linearly from 0.1 mm to 0.9–1.2 mm to values of 0.48–0.56, after which the apparent yield point is reached. Thereafter, μ of TM11 remains constant, for Sa6 it increases slightly, indicating minor strain hardening, and for TM6, TM7 and TM8 it decreases slightly with displacement, indicating minor strain weakening. We generally observe that for the high temperature experiments at 180°C , high clay contents (> 21 wt-%) lead to strain weakening (TM6, TM7, TM8), while strain hardening is observed for sample Sa6 with a clay content of ≤ 21 wt-%. TM11 which also has a clay content of ≤ 21 wt-% shows neither strain hardening nor weakening.

Figure 6 shows the final frictional coefficient, which is a mean of the friction coefficients over the last 0.4 mm displacement, versus clay content of the gouge (a) and the relative sampling position of the gouge in the fault (b). Friction coefficients range from 0.49 for sample TM7 to 0.60 for sample TM11 at 18°C . At 180°C , they seem to decrease with increasing clay content from 0.61 at 20 wt-% clay for Sa6 to 0.49 at 25 wt-% for TM7 (see

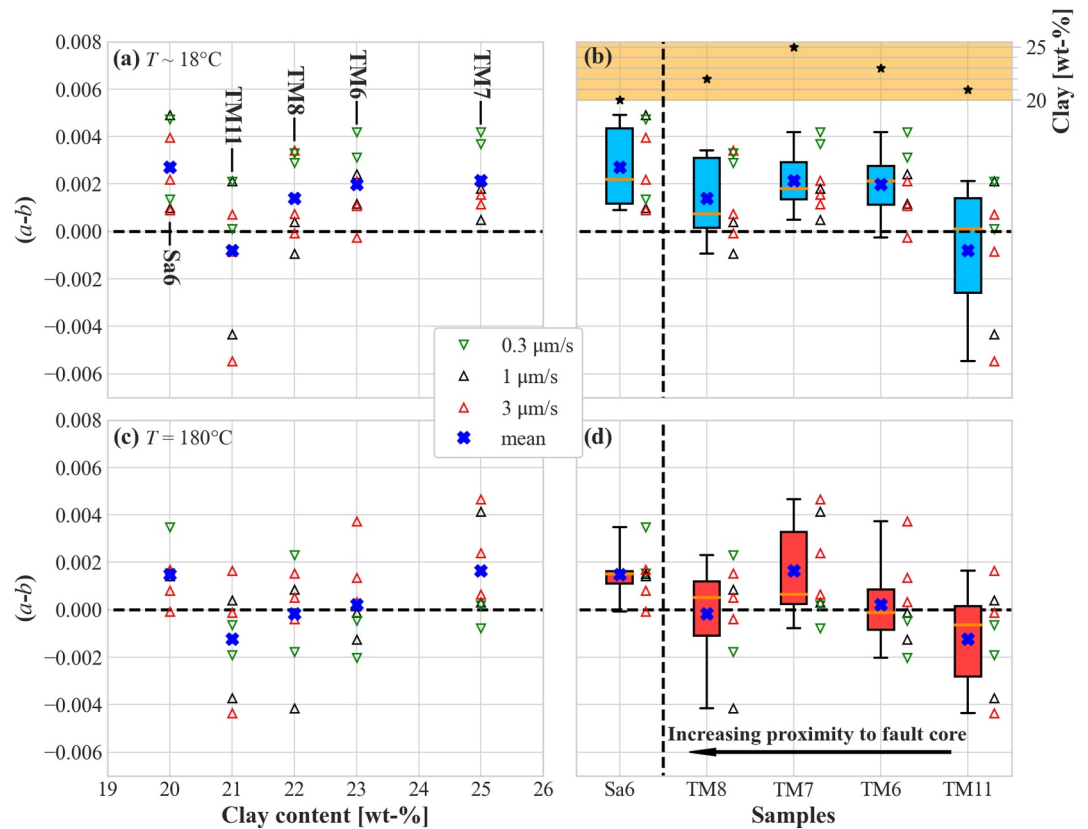


Figure 7. Frictional stability ($a - b$) against phyllosilicate content (left column) and ordered by proximity to fault core (right column) at room temperature ($\sim 18^\circ\text{C}$; top) and at high temperature (180°C ; bottom). Blue crosses represent mean values. Boxplots show mean value (blue cross), median (orange line), upper and lower quartile (box) and overall data range (whiskers) for data of each sample.

Figure 6a). This trend, however, is not supported by the low temperature data. TM11, TM6 and TM7 show that clay content increases while friction coefficient decreases with increasing proximity to the fault core (see Figure 6b). TM8 was collected from within the fault core but shows final friction coefficients at low and high temperature which are higher than for TM7, the next sample further away from the core.

Figure 7 relates the frictional stability of our samples to their clay content (a, c) and to their relative position to the fault core (b, d). The combined parameter ($a - b$) at low temperature (Figure 7a) ranges from -0.0057 to 0.0049 . The relatively low b values of Sa6 (20 wt-% clay) result in ($a - b$) values that are on average higher than for the other samples. Values of ($a - b$) for Sa6 are all positive and thus indicate VS behavior. Excluding sample Sa6, ($a - b$) increases with increasing clay content. TM11 (21 wt-% clay) shows both VS and VW behavior with values from -0.0057 to 0.0022 . Values of ($a - b$) range from -0.0012 to 0.0035 and -0.0003 to 0.0043 for samples TM8 and TM6 with 22 wt-% and 23 wt-% clays, respectively, indicating increasing VS behavior with increasing clay content. The sample with the highest clay content (TM7, 25 wt-%) shows ($a - b$) values from 0.0003 to 0.0043 , that is, VS behavior at all velocities tested. Clusters related to post-step slip velocity can be recognized, where ($a - b$) at $3 \mu\text{m/s}$ are lowest and values at $0.3 \mu\text{m/s}$ highest. At 180°C (Figure 7c), the ranges and the means of ($a - b$) of all samples shifted to smaller and more negative values and with this toward more VW behavior. We generally observe increasing ($a - b$) values with increasing clay content at high temperature for TM samples. Furthermore, the mean frictional stability generally increases with increasing proximity to the fault core from -0.0008 to 0.0021 at low temperature (Figure 7b) and from -0.0013 to 0.0017 at high temperature (Figure 7d).

3.2. Gouge Microstructures

In the following we describe the main characteristics of the gouge microstructures of all our samples at room temperature and of TM11, TM7 and Sa6 at high temperature. An overview and some example microstructures are

given in this chapter, but more detailed images, as well as EDS-element-maps are attached in Supporting Information S1. We use the terminology of Logan et al. (1992) in the description of the main shear structures.

Unaltered sample TM11: Figure 8a shows compressed but unsheared TM11. This was analyzed to study the sample microstructure before and after shear deformation. The homogeneously distributed large clasts (<125 μm) are mostly quartz, albite, and orthoclase with occasional larger interparticle booklets of muscovite and biotite. In addition, we find other small clay minerals like kaolinite and smectite and small amounts of apatite and rutile, while the latter is forming needles of 10–20 μm in length. Elongated and platy grains partly orient between $\sim 75^\circ$ and 90° (normal) to the compression direction. Biotite and muscovite predominantly orient perpendicular to normal stress and partially form layers around larger clasts.

In comparison, the sheared TM11 sample contains significantly fewer clasts of larger size compared to the unsheared counterpart (Figure 8b). This makes it more heterogenous with respect to spatial grain size distribution and causes the formation of specific shear structures, of which examples are shown in Figure 9. Large clasts are mostly quartz, while feldspars (albite and orthoclase) are widely fractured leading to a decrease in grain size. Shear deformation did not only lead to grain size reduction but also to generally rounder grains as a result of wear (Figures 9b and 9c). Some clasts roughly align and orient along early P-shears. Biotite and muscovite booklets, that aligned perpendicular to the compression direction in the unsheared sample, partially maintain previous layers they formed around larger clasts while others have been crushed between larger and stronger grains. Most micas orientate in the direction of P-foliation and R1-Riedel-shears (Figure 9c). Furthermore, the shearing has crushed apatite crystals that form “tails” (Figure 9d). These tails are crushed grains that align along the shear sense. Larger clasts are surrounded by fine to very fine-grained (<20 μm) matrix which concentrates in dedicated “deformation bands” and are lower in visible porosity compared to areas where larger grains dominate. Such deformation bands are found at the top and at the bottom of the gouge, indicating the formation of boundary Y-shears (Figure 8b), but are also along R1-shears (Figure 9a) where they promote the formation of fractures. Neither P-foliation nor R1-shears are very obvious throughout most of the sample. However, the gouge fractured along some R1-shears (Figure 9a) and R1- and P-orientation are indicated in mineral orientation and alignments.

TM11 sheared at 180°C: The structure of the unaltered granite gouge TM11 tested at 180°C differs significantly from the experiment performed at room temperature (Figure 8c). Like for the low temperature test, it contains large grains in a small-grained matrix. However, large grains are much less abundant, suggesting grinding to form smaller particles. Here, quartz and K-feldspar are fractured, while mainly fracturing of K-feldspar was observed for the low temperature experiment. The overall structure displays the shear sense well due to an easily identifiable P-foliation indicated by orientated and curved micas and apatite tails. The orientated and slightly ground micas form planes of weakness that promote fracture formation along shears. The P-foliation tails off into boundary Y-shears toward the top and the bottom of the gouge layer. In this gouge, P-foliation and Y-shears are dominant while R1-shears are present but less developed. The shear structures are more comparable to the more altered samples described below (e.g., TM7) than to room temperature TM11.

TM6 sheared at room temperature: The gouge of TM6 (Figure 8d) is less dominated by larger grains than TM11. The large grains are K-feldspar and quartz, with some larger booklets of mica. EDS-mapping indicates small amounts of albite in the fine-grained matrix indicated by elevated Na^+ concentrations. The P-foliation is composed of orientated and bent micas as well as orientated elongated grains. It is most obvious in the central part of the gouge, interbedded between horizontal boundary Y-shears. The latter take the form of deformation bands, dominated by an accumulation of smaller grains. TM6 contains brighter areas in the central part of the gouge that can be identified as crushed K-feldspar.

TM7 sheared at room temperature: The gouge made from TM7 is highly altered and is characterized by the highest clay content of all samples tested (Figure 8e). This results in a significantly different gouge structure in comparison to TM11. It contains less larger grains (quartz, rounded or fractured K-feldspar) that are surrounded by a fine-grained matrix. EDS-mapping shows little Na^+ within the gouge which confirms the XRD results suggesting small amounts of plagioclase. Muscovite is partially ground to form particles <50 μm (some forming “tails” like apatite) and either orientated normal to stress direction or forming oscillating P-foliations. Al^{3+} in the EDS maps further indicates that the P-foliation contains higher amounts muscovite and illite compared to surrounding areas. Only small amounts of biotite are found in TM7, suggesting dissolution, transformation into chlorite, or grinding to fine particles. The fine-grained matrix in TM7 is dominated by pervasive P-foliation rather than distinct shears. P, R, and Y-shear structures developed more localized in the sheared TM11 gouge. Like for

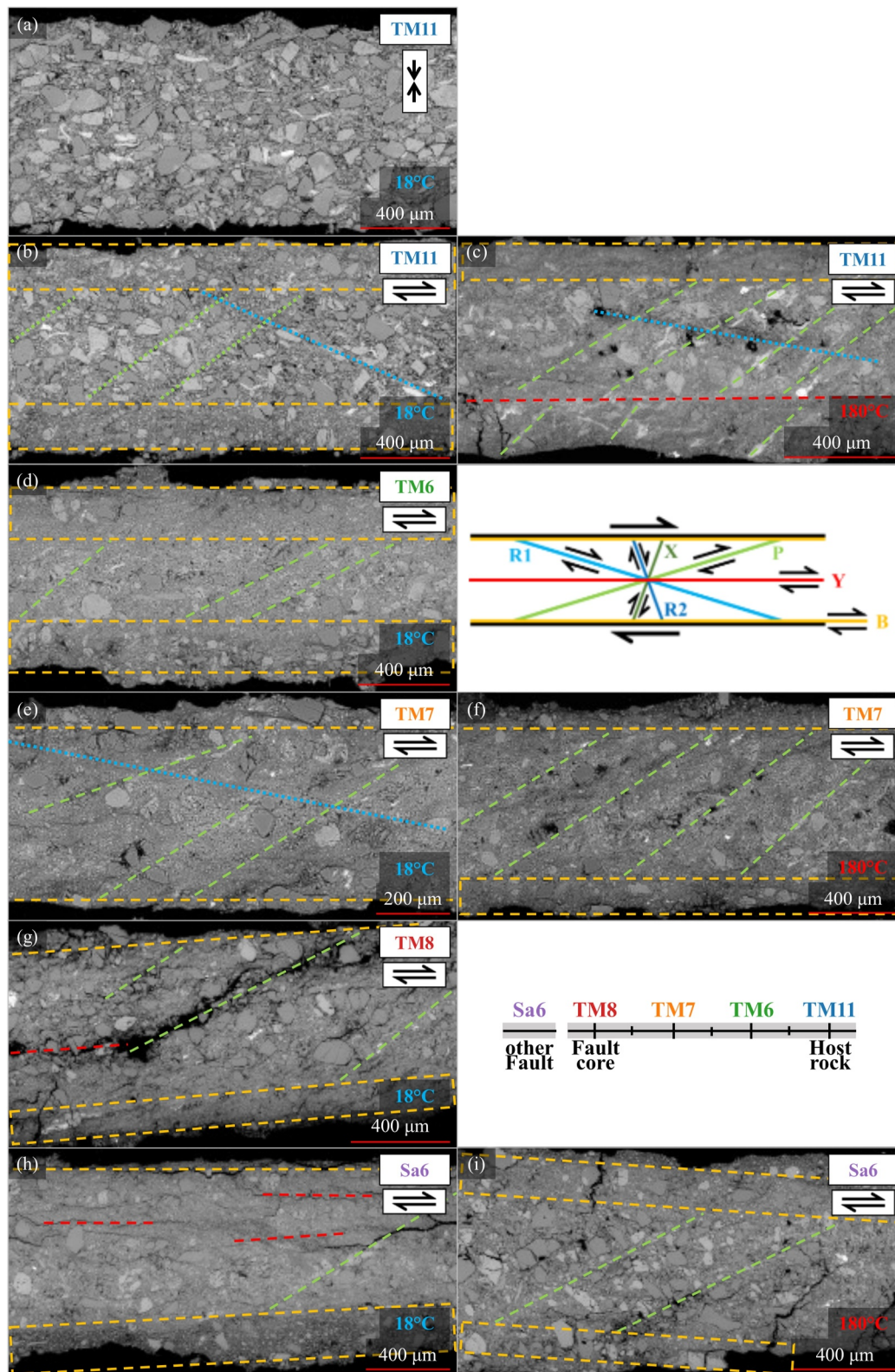


Figure 8. Scanning-Electron Microscopy images of gouges following experiments. Sample ID, shear sense and test temperature are indicated on the right side of each image. The gouge in panel (a) was only compressed without lateral displacement. Next to (d), a schematic describes typical shear structures as defined by Logan et al. (1992) adding B for boundary Y-shears. With a color code that is then used in the pictures to mark the related structures. Next to (g), a schematic indicates the relative origin position of the samples in the fault.

TM11, the boundary Y-shears in TM7 form toward the upper and lower boundary of the gouge, while fractures have formed along P- and R1-shears. In general, the SEM image shows brighter and darker areas; their distribution highlights the anastomosing foliation in the gouge structure. Brighter minerals are related to high K-feldspar contents following grinding to smaller particles. In comparison, porosity is filled with a less dense epoxy resin, leading to generally darker colors. As such, the SEM image appears darker toward the center of P-, R1-, and Y-shears which is potentially related to a concentration of clays and slightly higher porosity due to the onset of fracturing.

TM7 sheared at 180°C: In contrast to TM11, the structure of TM7 sheared at 180°C (Figure 8f) is very similar to the structure following the room temperature test on TM7. The big grains are slightly more damaged and more mid-sized grains are present at high temperature. The bright and dark zones described in TM7 are slightly more obvious, indicating shear direction and grain displacement. The undulating P-foliation fabric described before at low temperature is more defined at high temperature due to the more obvious P-foliation. This is because clays are generally better oriented, leading to the development of more bright zones.

TM8 sheared at room temperature: The fault core sample TM8 contains almost twice as much quartz as the other samples. Therefore, the large grains in the sheared gouge are dominated by quartz with some minor amounts of K-feldspar (Figure 8g). As before, these are surrounded by a small-grained matrix. The large grain fraction is higher than in TM6 and TM7, and lower than in TM11. The dark gouge is likely caused by low feldspars and high quartz contents. Crushed apatite embedded within the dark gouge can be found, creating some brighter areas. Furthermore, very bright fine grains are present throughout the gouge, likely being hematite, resulting in a reddish coloration. Apatite indicates the shear sense by forming “tails” of crushed particles that follow the P-foliation. The gouge shows fracturing along the P-foliation and slightly darker traces have formed where the gouge expanded as these areas are more porous (darker). Orientated micas are important to identify shear structures in previous gouges. However, only few large pieces of muscovite are left, and biotite is completely absent. The oscillating P-foliation transitions into horizontal boundary Y-shears toward the upper and lower boundary of the gouge. While P- and Y-shearing is obvious, R1-shears are more difficult to identify because they mainly take the form of aligned grains.

Sa6 sheared at room temperature: The mineralogical composition of Sa6 is similar to TM7 but contains higher kaolinite and quartz contents. The gouge from Sa6 is more heterogeneous than TM7. The structure is similar to TM6, with a similar content of large grains (Quartz, K-feldspar), embedded in a small-grained matrix (Figure 8h). The feldspars are fractured and have started to disperse into the matrix. Apart from the variable grain size, the gouge also seems to contain more porous areas with distinct boundaries separating them from areas of low porosity. The matrix orientation appears chaotic, not clearly representing the imposed shear sense in contrast to the other gouges. Large grains orientate in both, P- and R1-direction but the gouge is mainly fractured along P- and Y-direction as planes of weakness. The most dominant shears have formed along the P-foliation, underlining sinistral shear sense.

Sa6 sheared at 180°C: The microstructure following shearing at high temperature shows quite similar structure to its low temperature equivalent (Figure 8i); however, shears are better developed. Unlike for TM7 and TM11, Sa6 shows a higher share of large grains in the high compared to the low temperature measurement. The matrix is less chaotic with elongated grains mostly oriented in direction of the P-foliation.

4. Discussion

4.1. Alteration Stage of Samples

Our samples were collected at increasing proximity from and within the core of a minor cross-course fault zone in the Carnmenellis granite and exhibit different stages of granite alteration (Table 1). Alteration of a host rock gradually increases toward the fault core which is likely caused by enhanced access to fluids circulating through the damage zone (Faulkner et al., 2010). In Carnmenellis granite the main alteration mechanism observed around cross-course structures is argillic alteration which implies the formation of clay minerals (mainly kaolinite and smectite) at the cost of plagioclase (e.g., Bevins et al., 2010). With time, due to sericitization, the kaolinite and smectite transform into more stable secondary white mica like illite (Cuadros, 2012). K-feldspar also degrades, showing signs of sericitization of the sodium-rich mineral cores, but this process acts slower than the alteration of plagioclase. Argillic alteration can be observed in samples Sa6, TM6, TM7 and TM8, clearly showing a reduction

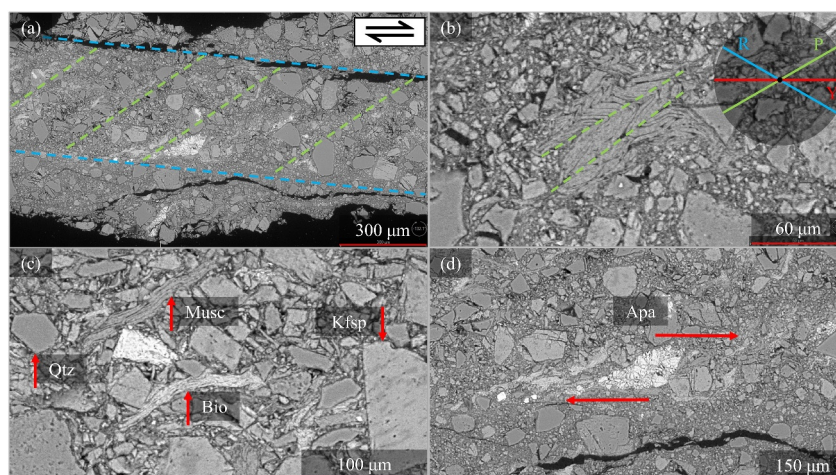


Figure 9. Examples for structural interpretation on sheared unaltered granite (TM11) at 18°C. (a) Overview of sheared unaltered gouge in which direction and approximate position of Riedel-shears (blue) and P-foliation (green) are marked with dotted lines. (b) Double folded muscovite with fold planes parallel to the direction of the P-foliation. Due to initially having been oriented against shear direction and the relatively low strength of the mica compared to quartz or feldspar minerals, the grain is folded rather than rotated. (c) Platy biotite (Bio) and muscovite (Musc) arranging toward P-foliation next to quartz (Qtz) and K-feldspar (Kfsp) grains. The feldspar contains darker lines indicating perthitic unmixing. (d) Soft apatite grains ground to smaller particles due to shear, forming “tails” with shape defined by the shear sense.

in plagioclase with an increase in kaolinite, smectite and chlorite in comparison to TM11 (see Table 1). In addition, the mafic minerals in the rock are transformed into chlorite. In Carnmenellis granite, this affects mainly biotite which is found in addition to or replaced by chlorite in more altered aggregates (Charoy, 1986). As a consequence, our samples show a significant loss in muscovite, biotite and illite from the unaltered (TM11) to the altered state by at least 5 wt-%. As muscovite is relatively stable under hydrothermal conditions and illite successively forms with time, the main mineral lost is biotite - either transforming into chlorite or lost in solution.

As a consequence of transformation of tectosilicates into phyllosilicates, the overall rock strength decreases and porosity increases (Coggan et al., 2013). It should be noted that porosity can only increase until alteration causes major parts of the rocks mineral structure to break down. At this point compaction can occur which reduces the pore space again. The TM samples become successively more altered with proximity to the fault core. From TM11 (furthest away from core) to TM8 (from within core), the amount of plagioclase decreases while the amount of clay minerals increases.

TM8 shows a small reduction in overall phyllosilicate and a significant increase in quartz content (59 wt-% see Table 1). One possibility to explain the reduction of clay and higher proportion of quartz in TM8 relative to all other samples is the removal of small clay particles associated with circulation of fluids along the fault. Alternatively, the fault could have hosted a quartz vein before shearing which would also increase the amount of quartz in the fault gouge. There was no obvious evidence for the presence of a former quartz vein in this fault, but it is also difficult to identify small quartz veins in heavily altered rock, especially after shear displacement. Furthermore, quartz veins are commonly present in cross-course structures (Bevins et al., 2010). Either explanation or even a combination of both appear reasonable. Sa6 was collected at a different fault in the same mine and based on the amount of plagioclase, it would be positioned in an alteration stage between TM7 and TM8. However, the combined amount of clay (kaolinite + smectite + chlorite) in Sa6 is relatively low and the fact that it contains most kaolinite in all samples makes a position toward the less altered end possible (e.g., between TM11 and TM6).

4.2. Frictional Strength and Stability of Altered Granite

The alteration sequence with proximity of our samples to the fault core is partly reflected in the final friction coefficients measured (Figure 6). Notably, the least altered sample TM11 showed the highest final friction coefficient (~0.6), while the lowest final friction coefficient of ~0.49 was exhibited by TM7, the second closest to the core. Fang et al. (2018a) analyzed the frictional behavior of natural and synthetic rocks with variable

composition and clay content. They reported that frictional strength decreases with phyllosilicate content and increases with tectosilicate content which is similar to observations made on artificial gouge mixtures with variable amounts of clay (e.g., Crawford et al., 2008; Takahashi et al., 2007; Tembe et al., 2010). In our experiments, we make similar observations for TM11, TM6 and TM7, showing the lowest final friction coefficient for TM7, containing the highest phyllosilicate content of 25 wt-%. However, the final friction coefficients observed for the other samples are not in full agreement with a decrease in the friction coefficient with an increase in phyllosilicate content. This may be related to the narrow range in phyllosilicate content in our samples (20–23 wt-%). Behnken and Faulkner (2012) analyzed the frictional behavior of different pure sheet silicates and found that at an effective pressure of 90 MPa, pure muscovite has a higher friction coefficient at the yield point than kaolinite, illite or smectite. Micas in TM11 are mostly muscovite and biotite due to the unaltered stage of the sample while the more altered samples contain increasing amounts of illite. This supports the higher friction coefficient of TM11 even though it contains a higher amount of phyllosilicates than Sa6.

Sa6 and TM6 (intermediate alteration) show similar frictional behavior at room temperature with the difference that Sa6 shows strain weakening behavior, and TM6 shows strain hardening. The main difference between these two samples lies in the phyllosilicate composition. While the amount of combined muscovite, biotite and illite is relatively similar, Sa6 contains more kaolinite and TM6 contains more chlorite and smectite. This does not seem to explain the observed strength difference as (a) Behnken and Faulkner (2012) found that pure kaolinite gouge has an almost three times higher friction coefficient at the yield point than pure smectite and (b) Tembe et al. (2010) found that an increase in the smectite content rather than the total clay content relates to lower friction coefficients. We hypothesize that this inconsistency is caused by the small differences in clay contents of our samples, which is reflected in only small differences in friction coefficients.

Keeping in mind the small differences in friction coefficients between the samples, we generally find that, at high temperature, frictional strength seems to decrease with increasing clay content across all samples. In the low temperature tests, Samples Sa6 and TM8 deviate from this trend with clay content. While these differences in friction coefficients at high and low temperature might lie well in the range of sample variability, we still want to discuss potential explanations to explore parallels to trends found in other studies. The shift from no clear trend at low temperature to a potential trend with clay content at high temperature could be caused by quartz and the feldspars in wet systems becoming more susceptible to thermally activated deformation mechanisms with increasing temperature (like stress corrosion cracking (SCC) and pressure solution, e.g., den Hartog & Spiers, 2014). When the previously strong tectosilicates become easier to shear and break, there is less dilatational movement between grains necessary to accommodate horizontal shear (den Hartog & Spiers, 2013; Niemeijer & Spiers, 2007). Rather than moving grains relative to other grains potentially causing lateral movement, the grains can deform or break. The weaker the tectosilicates become, the more the friction on horizontal clay minerals will contribute to the shear strength of the gouge. This shift in contribution to shear strength at high temperature could then also explain the trend of frictional strength with clay content in our high temperature tests.

Another possible effect of high temperature in granite friction we potentially see in our samples (e.g., TM6, TM7 and TM8) is a reduction of frictional strength with increasing temperature. While the frictional strength of TM11 stays almost the same and TM7 shows only a very small reduction, Sa6 shows a significant increase in frictional strength from low to high temperature. A potential reason relates to the friction against displacement curve that records the high temperature experiment on Sa6 (Figure 5b). In contrast to all other curves, the friction coefficient of Sa6, that reached steady-state conditions below 2.5 mm displacement, starts to divert from this state at a displacement of 2.5 mm, as the friction coefficient increases, and the frictional resistance starts to oscillate with displacement. To analyze the potential origin of this oscillation we looked at the recorded pressures, the temperature, the axial displacement rates, and the pump volumes. None of them showed cyclic behavior with displacement like the friction coefficient. A quick permeability test following the experiment also showed the sliders to be permeable, ruling out pore pressure build-ups during deformation. As we did not observe any machine related effect, we assume the oscillation could have been caused by spatial variations in the microstructure, maybe due to periodic formation and dispersion of force chains. However, proving that is difficult as we only analyze the microstructure at the end of the experiment.

Frictional stability shows the opposite behavior compared to the frictional strength for our alteration sequence (Figure 7). ($a - b$) and thus, frictional stability is VW for TM11 that was sampled the furthest from the fault core and then becomes VS with increasing proximity to the fault core for Sa6, TM6, and TM7. In TM8, which was

sampled from within the fault core, $(a - b)$ decreases slightly. This can again be related to higher amounts of quartz in the sample caused by an additional process. When trying to relate the frictional stability behavior to the overall clay content, TM11, TM6, TM7, and TM8 also seem to form a trend toward higher $(a - b)$ values with higher phyllosilicate content. This observation agrees with previous work that reported a stabilizing effect of phyllosilicates on slip (e.g., Fang et al., 2018; Ikari et al., 2011; Tembe et al., 2010). Again, Sa6 is not consistent with this trend as it only shows VS behavior while having the lowest phyllosilicate content.

In the high temperature tests, frictional stability again changes from VW from TM11 to VS toward the fault core for Sa6, TM6, and TM7 while decreasing slightly for the core sample TM8. This is the same behavior of the altered samples compared to their low temperature equivalent, indicating that the same or at least similar processes control frictional stability at both temperatures. Previous work reports that $(a - b)$ of granular gouges decreases with increasing temperature, changing from VS to VW behavior where the trend turns and then increases with further increase in temperature, back from VW to VS behavior (e.g., Blanpied et al., 1998; den Hartog & Spiers, 2013). This creates a VW temperature window that Blanpied et al. (1998) reported for wet granite gouge at a temperature range between $\sim 90^\circ\text{C}$ and $\sim 350^\circ\text{C}$. The exact temperature limits of the window vary dependent on other conditions (see den Hartog & Spiers, 2013), but our results are in general agreement with the observations as the frictional stability for all of our samples is reduced at 180°C compared to the room temperature tests. This leads to a more velocity neutral and for some even VW behavior, which is related to less stable sliding and a higher potential for stick slip behavior.

4.3. Gouge Structure and Frictional Behavior

Argillic alteration is the main process relevant for our suite of samples, by which large feldspar crystals are replaced by clay particles. This can be seen in the grain size distributions of the increasingly altered samples (TM6, TM7) containing more smaller grains than the less altered sample (TM11, quantitative structural analysis in Supporting Information S1). This suggests that, in addition to the phase change, argillic alteration also indirectly causes a significant reduction in grain sizes, which is affecting frictional behavior (e.g., Anthony & Marone, 2005; Bedford & Faulkner, 2021; Higashi & Sumita, 2009; Jiang et al., 2016; Mair et al., 2002). Bedford and Faulkner (2021) tested the effects of grain size on shear localization and sliding behavior on quartz powders of different initial grain sizes between 40 and 120 MPa normal stress. They report that the smaller the initial grain size of the gouge, the more deformation will localize, and unstable sliding will become more likely. We cannot report this size effect in our test, but we also observe localization of shear in our samples.

Although grain sizes are larger, the sheared unaltered sample (TM11) contains zones where smaller grains accumulate toward the boundaries, indicating the beginning of formation of boundary Y-shear zones (Figure 8b). In comparison, grain sizes in the more altered samples (TM6, TM7) are homogeneously distributed over the gouge layers, and shearing affects the width of the gouges more evenly (Figures 8c and 8d), dispersing deformation over a larger volume. This difference in localized boundary shearing in the unaltered sample against pervasive layer deformation in the altered samples is a first effect promoting more stable sliding in our altered samples. However, this is opposite to Bedford and Faulkner (2021) who reported smaller grain sizes to promote shear localization and less stable sliding. A potential explanation of this difference to Bedford and Faulkner (2021) could be the initial maximum grain sizes of their samples of 5–30 μm . As we start from a significantly larger maximum grain size of 125 μm , more strain is needed to accommodate similar degrees of localization.

In addition to the grain size effect on localization, grains that align toward R1-shears form force chains over the thickness of the gouge layer. The development characteristics of these chains were also found to affect frictional properties (e.g., Anthony & Marone, 2005; Jiang et al., 2016). As the unaltered material contains fewer large grains over the same thickness compared to the altered material, the force chains can accommodate higher stresses, for which a stress release (e.g., due to mechanical failure of a grain in the chain) is related to less stable sliding (Anthony & Marone, 2005). In contrast, the force chains in the altered material need to consist of significantly more grains to span the same layer thickness as the unaltered material. Anthony and Marone (2005) report, that such chains, composed of more, smaller grains, are weaker and more compliant to deformation. Stresses cannot build up as high and creep in the gouge happens more stably.

The development of friction parameters and microstructure are further affected by the chemical phase transformation from feldspars to clays which increases the clay fractions in the gouge. An increase in clay fraction has been found to stabilize sliding at fixed conditions (e.g., Ashman & Faulkner, 2022; den Hartog & Spiers, 2013;

Fang et al., 2018; Ikari et al., 2011; Tembe et al., 2010). With the phase change, the large feldspar grains are replaced by small platy clay grains. Although there are only small differences in the grain aspect ratios of our samples, the more altered rocks (TM6 and TM7) show tendencies toward more elongated grains than the least altered sample (TM11, see Supporting Information S1). These elongated clays promote the formation of foliations and clay shear fabrics, which initially stabilize shear and allow easier orientation of grains in the direction of major shear structures. This is due to the low bond strength between the phyllosilicate sheets whose separation may further suppress dilatancy in the material (Ikari et al., 2011).

In our experiments, we see more distinct preferred grain orientation in the direction of shear structures from least altered (TM11), over the intermediate altered (TM6 and Sa6), to the most altered stages (TM7 and TM8). Outside the fault core, the long axes of the grains orient clearer to shear structures with a higher degree of alteration (in the order of TM11 to TM6, and TM7), indicating an increase in pronounced shear fabrics. The least altered sample (TM11) contains the lowest amount of clays and shows orientations that are most independent of shear structures and closest to simple compression. The more altered the sample, the broader the grains orientate away from horizontal compression and toward P- and R1-shear directions (see TM6). The formation of pervasive undulating P-foliation fabric with shear is promoted for samples with higher clay content (Figure 8c). Finally, the sample containing the most clays (TM7) also contains the most distinct grain orientations toward P- and B/Y-orientation (see quantitative analysis in Supporting Information S1). In this sample the fabric is most developed, stabilizing sliding and decreasing frictional strength compared to TM11. The estimated porosity based on black values in the SEM images is lowest, hinting to least dilatational shear. As a result, we see the present argillic alteration promoting anisotropy of gouges by promoting the formation of shear fabrics and foliation, and with further displacement promoting formation of shear structures.

The fault core sample (TM8) diverges from the trends we found for the frictional behavior from TM11 (unaltered) to TM7 (close to core). As reported earlier, TM8 contains the highest amount of quartz for all our samples because of an additional process. This affects the grain size distribution, as the relative amount of stronger and potentially larger grains is increased while the relative amount of small clay particles is reduced. In addition to the size effect, the quartz grains are more rounded than clays and feldspars (also visible in aspect ratios analyzed in Supporting Information S1) and cause more evenly distributed grain-orientations than in the sample with the highest clay content (TM7). However, shear structures and clay fabric are still relatively well developed in the fault core sample (TM8) in comparison to the unaltered sample (TM11) due to the higher amount of small-grained matrix. This also affects frictional strength because the force chain network will develop similar to the other altered samples (TM6 and TM7). However, the fabrics are more localized in TM8 than in TM7, anastomosing around other grains and causing less stable sliding and higher frictional strength. In conclusion, larger quartz grains are probably responsible for higher strength and the less stable sliding than in the other highly altered sample (TM7), but sliding is still more stable in the fault core sample than in the unaltered sample (TM11) due to the larger proportion of clays.

A comparison of gouge samples from low and high temperature tests shows for the unaltered sample (TM11) that the post shear grain size distributions at high temperature contain more smaller grains and that the grains are more oriented toward the major shear structures. The difference in grain size could be related to granite becoming weaker with increasing temperature (e.g., Yin et al., 2016). This could indicate that during shear at higher temperatures more brittle failure occurs, generally resulting in more smaller grains. As this is simple grain size reduction without a phase transition (as it would be caused by argillic alteration), such a reduction promotes shear localization and with this less stable sliding (e.g., Bedford & Faulkner, 2021). In contrast to the unaltered sample (TM11), this effect of temperature is not as visible in the high clay sample (TM7) because the grain sizes are mostly similar after shearing at low and the high temperature. However, the narrower distribution of orientations of grains in the 180°C gouge hint at a more developed fabric/foliation which could then cause more localized shear and therefore less stable sliding (see quantitative analysis in paper supplements).

The effects of temperature on the frictional behavior have formerly been related to the competition of different microstructural processes. Niemeijer and Spiers (2007) explain temperature driven changes in friction in halite-muscovite mixtures by the competition of thermally activated compaction and granular flow causing dilation, for which temperature controls the mechanism that dominates deformation. In their three-regime-model pressure solution is suggested as thermally activated compaction mechanism. den Hartog et al. (2012) applied the Niemeijer and Spiers (2007) model to their experiments on crushed illite-rich Rochester shale and found close

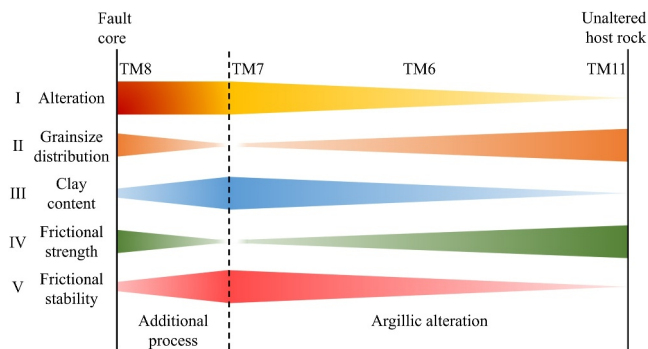


Figure 10. Schematic of the implications of our results on frictional behavior. The wider the beam: (I) the more developed the rock alteration state, (II) the higher the amount of large grains, (III) the higher the clay content, (IV) the higher frictional strength and (V) the higher frictional stability. The color change in alteration (I) represents an additional process necessary to explain frictional changes toward the fault center.

resemblance to their observed temperature dependence of friction and microstructure. However, den Hartog et al. (2012) also state that pressure solution would be insufficient to accommodate the required compaction at high temperatures under their used conditions. They suggest thermally activated SCC as dominant deformation process in their experiments. The grainsize distributions in our high temperature tests are shifted to smaller grainsizes compared to our room temperature equivalents which could imply a contribution of a thermally activated deformation mechanism. Similar to den Hartog et al. (2012), we assume that pure pressure solution would be insufficient to accommodate shear deformation under our used conditions as we see no evidence for it in our microstructures. Although we observe tailed apatite clasts in our samples, the tails consist of crushed material and show no signs of dissolution or precipitation. The feldspars and quartz grains are more fractured, more angular, and smaller in our high temperature gouges which would imply SCC as acting process.

4.4. Implications for Fault Behavior in Geothermal Settings

Our room temperature results suggest that geochemical alteration stabilizes slip in granitic fault systems. The closer the proximity to the fault core, the more altered it is likely to be, reducing frictional strength but increasing frictional stability (see TM11, TM6, and TM7 in Figure 10). A granitic gouge that initially exhibits VW behavior is expected to shear more stably if plagioclase is replaced by clays, but due to the reduced strength, shear also becomes more likely. As more stable shear means a decrease in the likelihood of stick-slip events which are related to seismicity, shearing in more altered material is more likely to happen aseismically, contributing to destressing the system with less seismicity. The increase in clay content due to argillic alteration also promotes the formation of shear fabrics and therefore the orientation of grains. These fabrics potentially make fault gouge more anisotropic and affect other physical and hydraulic properties (Kenigsberg et al., 2019; Kenigsberg et al., 2020).

We further found the trends with alteration to still be valid at up to 180°C, which is comparable to the bottom hole temperature at the UDDGP project. However, if alteration continues and additional processes reduce the amount of clays (like the integration of a quartz-vein or loss of fines due to flow along the), the remaining gouge will be enriched in stable grains like quartz (TM8). This could reduce fault stability over longer time scales. This accumulation of stable grains is limited by the fault permeability. A lower permeability will reduce overall geochemical reactions (i.e., dissolution and precipitation) by providing less fluid that is out of equilibrium with the host rock. Furthermore, fault stability is also controlled by the strength of the rock surrounding the core. If this rock is weaker due to higher amounts of clay, then slip and deformation will be concentrated where the rock is the weakest. The potential effects of temperature on fault friction were reported earlier (e.g., Blanpied et al., 1998; den Hartog & Spiers, 2013). Our findings mainly support these, as our tests at higher temperature showed sliding to become less stable from low temperature toward the VW window, while frictional strength decreased as well. Temperature had a similar effect on all samples, regardless of the composition, that is, a higher or lower degree of alteration does not enhance or dampen any temperature effects. In turn this general temperature related shift of our data suggests that the stabilizing effect of alteration on frictional stability is temperature independent, because the magnitude of the increase in stability with increasing alteration (from TM11, over TM6 to TM7) is about the same for our low and high temperature tests.

With respect to the UDDGP project and its suspected temperature range from 80 to 180°C from injection to production well, the injection of new fluids or the reinjection of produced fluids could trigger further argillic alteration as it usually occurs between 100 and 300°C (Pirajno, 2009). Although the overlap of these temperature ranges does not include the 80°C at the injection well, related lower temperature processes like kaolinization (Psyrrillos et al., 2003) will have the same effect of replacing feldspars with clay minerals closer to the injection well. Over longer periods of time, this can then widen the alteration zones around conductive faults and gradually reduce frictional strength while increasing frictional stability. Assuming a wider alteration zone also means a wider fault or potentially thicker fault gouge layer involved in the accommodation of displacement, this widening has an additional stabilizing effect as thicker gouge layers were found show more stable shearing than thin ones (Byerlee & Summers, 1976; Marone et al., 1990).

5. Conclusions

A series of direct shear experiments at room temperature and in situ pressure conditions were conducted on granite gouges to investigate the effects of chemical alteration on the frictional behavior in granitic fault systems. We used Carnmenellis granite samples from a fault (cross-course structure) in Cornwall that exhibit different degrees of natural alteration. Samples that underwent a higher degree of alteration show higher amounts of clay minerals (kaolinite, smectite, chlorite) and lower amounts of plagioclase. Frictional strength of the samples decreases with increasing proximity to the fault core except for the sample closest to it. The sample collected from within the fault core contains higher amounts of quartz in comparison to the other samples which we relate either to removal of other minerals dissolved as small particles in fluid or the integration of material from a small quartz vein into the gouge. Frictional stabilities of the samples change from velocity-weakening in the least altered sample to velocity-strengthening in the more altered samples. The fault core sample shows less velocity-strengthening behavior than two less altered samples, presumably due to the increase in quartz content. Microstructural analysis of the samples relates alteration and increasing frictional stability to delocalization of shear fabrics due to reduction of grain size and increase in clay content. Tests at 180°C showed a general decrease in sliding stability compared to the low temperature tests, while the intensity of the decrease was independent of alteration stage. From our results we suggest that argillic alteration around faults generally increases the likelihood of slip to occur but stabilizes slip toward the fault core, destressing the system by promoting aseismic shear. However, additional effects of altered or dissolved material may complicate this pattern.

Conflict of Interest

The authors declare no conflicts of interest relevant to this study.

Data Availability Statement

The data that supports the findings of this study are available within the article and the Supporting Information S1. Raw friction data as well as the Rate-and-State-Friction parameters analyzed are available at Harpers et al. (2024).

Acknowledgments

This work was done in collaboration with the GWatt project led by the British Geological Survey (BGS) and funded by United Kingdom Research and Innovation (UKRI) through the Natural Environment Research Council (NERC) under NE/S004769/1. It would not have been possible without Chris Yeomans who helped to collect the sample material and shared his knowledge on the geology of Cornwall. We would also like to thank Paul Miller for helping with sample preparation.

References

- Abesser, C., Busby, J. P., Pharaoh, T. C., Bloodworth, A. J., & Ward, R. S. (2020). *Unlocking the potential of geothermal energy in the UK, Rep.* British Geological Survey.
- Anthony, J. L., & Marone, C. (2005). Influence of particle characteristics on granular friction. *Journal of Geophysical Research*, *110*(B8), B08409. <https://doi.org/10.1029/2004JB003399>
- Ashman, I. R., & Faulkner, D. R. (2022). *The effect of clay content on the dilatancy and frictional properties of fault gouge.* Authorea Preprints.
- Barrier, D., Ledesert, B., Clauer, N., Meunier, A., Liewig, N., Morvan, G., & Addad, A. (2008). Hydrothermal alteration of the Soultz-sous-Forêts granite (Hot Fractured Rock geothermal exchanger) into a tosudite and illite assemblage. *European Journal of Mineralogy*, *20*(1), 131–142. <https://doi.org/10.1127/0935-1221/2008/0020-1787>
- Bedford, J. D., & Faulkner, D. R. (2021). The role of grain size and effective normal stress on localization and the frictional stability of simulated quartz gouge. *Geophysical Research Letters*, *48*(7), e2020GL092023. <https://doi.org/10.1029/2020GL092023>
- Bedford, J. D., Faulkner, D. R., & Lapusta, N. (2022). Fault rock heterogeneity can produce fault weakness and reduce fault stability. *Nature Communications*, *13*(1), 326. <https://doi.org/10.1038/s41467-022-27998-2>
- Beeler, N. M., Tullis, T. E., Blanpied, M. L., & Weeks, J. D. (1996). Frictional behavior of large displacement experimental faults. *Journal of Geophysical Research*, *101*(B4), 8697–8715. <https://doi.org/10.1029/96JB00411>
- Behnken, J., & Faulkner, D. R. (2012). The effect of mineralogy and effective normal stress on frictional strength of sheet silicates. *Journal of Structural Geology*, *42*, 49–61. <https://doi.org/10.1016/j.jsg.2012.06.015>
- Bevins, R. E., Young, B., Mason, J. S., Manning, D. A. C., & Symes, R. F. (2010). Mineralization of England and Wales. In L. P. Thomas & E. L. Durham (Eds.), *Geological conservation review series, No. 36*. JNCC, Peterborough.
- Beynon, S. J., & Faulkner, D. R. (2020). Dry, damp, or drenched? The effect of water saturation on the frictional properties of clay fault gouges. *Journal of Structural Geology*, *140*, 104094. <https://doi.org/10.1016/j.jsg.2020.104094>
- Biegel, R., Wang, W., Scholz, C., Boitnott, G., & Yoshioka, N. (1992). Micromechanics of rock friction 1. Effects of surface roughness on initial friction and slip hardening in Westerly granite. *Journal of Geophysical Research*, *97*(B6), 8951–8964. <https://doi.org/10.1029/92JB00042>
- Bischoff, A., Heap, M. J., Mikkola, P., Kuva, J., Reuschlé, T., Jolis, E. M., et al. (2024). Hydrothermally altered shear zones: A new reservoir play for the expansion of deep geothermal exploration in crystalline settings. *Geothermics*, *118*, 102895. <https://doi.org/10.1016/j.geothermics.2023.102895>
- Blanpied, M. L., Lockner, D. A., & Byerlee, J. D. (1995). Frictional slip of granite at hydrothermal conditions. *Journal of Geophysical Research*, *100*(B7), 13045–13064. <https://doi.org/10.1029/95JB00862>
- Blanpied, M. L., Marone, C. J., Lockner, D. A., Byerlee, J. D., & King, D. P. (1998). Quantitative measure of the variation in fault rheology due to fluid-rock interactions. *Journal of Geophysical Research*, *103*(B5), 9691–9712. <https://doi.org/10.1029/98JB00162>
- Bos, B., Peach, C. J., & Spiers, C. J. (2000). Frictional-viscous flow of simulated fault gouge caused by the combined effects of phyllosilicates and pressure solution. *Tectonophysics*, *327*(3), 173–194. [https://doi.org/10.1016/S0040-1951\(00\)00168-2](https://doi.org/10.1016/S0040-1951(00)00168-2)

- Bott, M. H. P., Day, A. A., Masson-Smith, D., & Dunham, K. C. (1958). The geological interpretation of gravity and magnetic surveys in Devon and Cornwall. *Philosophical Transactions of the Royal Society of London - Series A: Mathematical and Physical Sciences*, 251(992), 161–191. <https://doi.org/10.1098/rsta.1958.0013>
- Busby, J., & Terrington, R. (2017). Assessment of the resource base for engineered geothermal systems in Great Britain. *Geothermal Energy*, 5(1), 7. <https://doi.org/10.1186/s40517-017-0066-z>
- Byerlee, J. D. (1967). Frictional characteristics of granite under high confining pressure. *Journal of Geophysical Research*, 72(14), 3639–3648. <https://doi.org/10.1029/JZ072i014p03639>
- Byerlee, J. D., & Summers, R. (1976). A note on the effect of fault gouge thickness on fault stability. *International Journal of Rock Mechanics and Mining Sciences & Geomechanics Abstracts*, 13(1), 35–36. [https://doi.org/10.1016/0148-9062\(76\)90226-6](https://doi.org/10.1016/0148-9062(76)90226-6)
- Chadwick, R. A., & Evans, D. J. (1995). The timing and direction of Permo-Triassic extension in southern Britain. *Geological Society, London, Special Publications*, 91(1), 161–192. <https://doi.org/10.1144/gsl.Sp.1995.091.01.09>
- Charoy, B. (1986). The genesis of the Cornubian batholith (South-West England): The example of the Carnmenellis pluton. *Journal of Petrology*, 27(3), 571–604. <https://doi.org/10.1093/ptrology/27.3.571>
- Chen, X., He, P., & Qin, Z. (2018). Damage to the microstructure and strength of altered granite under wet–dry cycles. *Symmetry*, 10(12), 716. <https://doi.org/10.3390/sym10120716>
- Chesley, J. T., Halliday, A. N., Snee, L. W., Mezger, K., Shepherd, T. J., & Scrivener, R. C. (1993). Thermochronology of the Cornubian batholith in southwest England: Implications for pluton emplacement and protracted hydrothermal mineralization. *Geochimica et Cosmochimica Acta*, 57(8), 1817–1835. [https://doi.org/10.1016/0016-7037\(93\)90115-d](https://doi.org/10.1016/0016-7037(93)90115-d)
- Coggan, J. S., Stead, D., Howe, J. H., & Faulks, C. I. (2013). Mineralogical controls on the engineering behavior of hydrothermally altered granites under uniaxial compression. *Engineering Geology*, 160, 89–102. <https://doi.org/10.1016/j.enggeo.2013.04.001>
- Crawford, B. R., Faulkner, D. R., & Rutter, E. H. (2008). Strength, porosity, and permeability development during hydrostatic and shear loading of synthetic quartz-clay fault gouge. *Journal of Geophysical Research*, 113(B3), B03207. <https://doi.org/10.1029/2006JB004634>
- Cuadros, J. (2012). Clay crystal-chemical adaptability and transformation mechanisms. *Clay Minerals*, 47(2), 147–164. <https://doi.org/10.1180/claymin.2012.047.2.01>
- Dearman, W. R. (1963). Wrench-faulting in Cornwall and south Devon. *Proceedings of the Geologists' Association*, 74(3), 265–287. [https://doi.org/10.1016/s0016-7878\(63\)80023-1](https://doi.org/10.1016/s0016-7878(63)80023-1)
- den Hartog, S. A. M., Niemeijer, A. R., & Spiers, C. J. (2012). New constraints on megathrust slip stability under subduction zone P–T conditions. *Earth and Planetary Science Letters*, 353–354, 240–252. <https://doi.org/10.1016/j.epsl.2012.08.022>
- den Hartog, S. A. M., & Spiers, C. J. (2013). Influence of subduction zone conditions and gouge composition on frictional slip stability of megathrust faults. *Tectonophysics*, 600, 75–90. <https://doi.org/10.1016/j.tecto.2012.11.006>
- den Hartog, S. A. M., & Spiers, C. J. (2014). A microphysical model for fault gouge friction applied to subduction megathrusts. *Journal of Geophysical Research: Solid Earth*, 119(2), 1510–1529. <https://doi.org/10.1002/2013jb010580>
- Dieterich, J. H. (1978). Time-dependent friction and the mechanics of stick-slip. In *Rock friction and earthquake prediction* edited. (pp. 790–806). Springer.
- Dieterich, J. H. (1979). Modeling of rock friction: 1. Experimental results and constitutive equations. *Journal of Geophysical Research*, 84(B5), 2161–2168. <https://doi.org/10.1029/JB084iB05p02161>
- Fang, Y., Elsworth, D., Wang, C., & Jia, Y. (2018). Mineralogical controls on frictional strength, stability, and shear permeability evolution of fractures. *Journal of Geophysical Research: Solid Earth*, 123(5), 3549–3563. <https://doi.org/10.1029/2017JB015338>
- Faulkner, D. R., & Armitage, P. J. (2013). The effect of tectonic environment on permeability development around faults and in the brittle crust. *Earth and Planetary Science Letters*, 375, 71–77. <https://doi.org/10.1016/j.epsl.2013.05.006>
- Faulkner, D. R., Jackson, C. A. L., Lunn, R. J., Schlische, R. W., Shipton, Z. K., Wibberley, C. A. J., & Withjack, M. O. (2010). A review of recent developments concerning the structure, mechanics and fluid flow properties of fault zones. *Journal of Structural Geology*, 32(11), 1557–1575. <https://doi.org/10.1016/j.jsg.2010.06.009>
- Faulkner, D. R., Sanchez-Roa, C., Boulton, C., & den Hartog, S. A. M. (2018). Pore fluid pressure development in compacting fault gouge in theory, experiments, and nature. *Journal of Geophysical Research: Solid Earth*, 123(1), 226–241. <https://doi.org/10.1002/2017jb015130>
- Forbes Inskip, N., Harpers, N., Shail, R., Claes, H., den Hartog, S., & Busch, A. (2023). *Reservoir properties of fault-related hydrothermally altered granites in Cornwall: Implications for geothermal energy prospectivity*. Authorea Preprints.
- Hadizadeh, J., Tullis, T. E., White, J. C., & Konkachbaev, A. I. (2015). Shear localization, velocity weakening behavior, and development of cataclastic foliation in experimental granite gouge. *Journal of Structural Geology*, 71, 86–99. <https://doi.org/10.1016/j.jsg.2014.10.013>
- Harpers, N., Forbes Inskip, N., Allen, M. J., Buckman, J., Faulkner, D. R., Claes, H., et al. (2024). Effects of chemical alteration on frictional properties in a deep, granitic, geothermal system in Cornwall: Direct shear experiments at near in-situ conditions (version 1) [Dataset]. *Zenodo*. <https://doi.org/10.5281/zenodo.12783984>
- He, C., Wang, Z., & Yao, W. (2007). Frictional sliding of gabbro gouge under hydrothermal conditions. *Tectonophysics*, 445(3), 353–362. <https://doi.org/10.1016/j.tecto.2007.09.008>
- Higashi, N., & Sumita, I. (2009). Experiments on granular rheology: Effects of particle size and fluid viscosity. *Journal of Geophysical Research*, 114(B4), B04413. <https://doi.org/10.1029/2008JB005999>
- Hunfeld, L. B., Niemeijer, A. R., & Spiers, C. J. (2017). Frictional properties of simulated fault gouges from the seismogenic groningen gas field under in situ P–T -chemical conditions. *Journal of Geophysical Research: Solid Earth*, 122(11), 8969–8989. <https://doi.org/10.1002/2017jb014876>
- Ikari, M. J., Marone, C., & Saffer, D. M. (2011). On the relation between fault strength and frictional stability. *Geology*, 39(1), 83–86. <https://doi.org/10.1130/g31416.1>
- Ishibashi, T., Elsworth, D., Fang, Y., Riviere, J., Madara, B., Asanuma, H., et al. (2018). Friction-stability-permeability evolution of a fracture in granite. *Water Resources Research*, 54(12), 9901–9918. <https://doi.org/10.1029/2018WR022598>
- Jiang, Y., Wang, G., Kamai, T., & McSaveney, M. J. (2016). Effect of particle size and shear speed on frictional instability in sheared granular materials during large shear displacement. *Engineering Geology*, 210, 93–102. <https://doi.org/10.1016/j.enggeo.2016.06.005>
- Kamila, Z., Kaya, E., & Zarrouk, S. J. (2021). Reinjection in geothermal fields: An updated worldwide review 2020. *Geothermics*, 89, 101970. <https://doi.org/10.1016/j.geothermics.2020.101970>
- Kenigsberg, A. R., Rivière, J., Marone, C., & Saffer, D. M. (2019). The effects of shear strain, fabric, and porosity evolution on elastic and mechanical properties of clay-rich fault gouge. *Journal of Geophysical Research: Solid Earth*, 124(11), 10968–10982. <https://doi.org/10.1029/2019JB017944>

- Kenigsberg, A. R., Rivière, J., Marone, C. J., & Saffer, D. M. (2020). Evolution of elastic and mechanical properties during fault shear: The roles of clay content, fabric development, and porosity. *Journal of Geophysical Research: Solid Earth*, *125*(3), e2019JB018612. <https://doi.org/10.1029/2019JB018612>
- Kilgore, B., Blanpied, M. L., & Dieterich, J. H. (1993). Velocity dependent friction of granite over a wide range of conditions. *Geophysical Research Letters*, *20*(10), 903–906. <https://doi.org/10.1029/93GL00368>
- Leclère, H., Faulkner, D., Wheeler, J., & Mariani, E. (2016). Permeability control on transient slip weakening during gypsum dehydration: Implications for earthquakes in subduction zones. *Earth and Planetary Science Letters*, *442*, 1–12. <https://doi.org/10.1016/j.epsl.2016.02.015>
- Ledingham, P., Cotton, L., & Law, R. (2019). The united downs deep geothermal power project. In *Paper presented at 44th Workshop on geothermal reservoir engineering*. Stanford University.
- Logan, J. M., Dengo, C. A., Higgs, N. G., & Wang, Z. Z. (1992). Chapter 2 fabrics of experimental fault zones: Their development and relationship to mechanical behavior. In B. Evans & T. F. Wong (Eds.), *International geophysics* (pp. 33–67). Academic Press.
- Mair, K., Frye, K. M., & Marone, C. (2002). Influence of grain characteristics on the friction of granular shear zones. *Journal of Geophysical Research*, *107*(B10), 2219. <https://doi.org/10.1029/2001JB000516>
- Marone, C. (1998). Laboratory-derived friction laws and their application to seismic faulting. *Annual Review of Earth and Planetary Sciences*, *26*(1), 643–696. <https://doi.org/10.1146/annurev.earth.26.1.643>
- Marone, C., Raleigh, C. B., & Scholz, C. H. (1990). Frictional behavior and constitutive modeling of simulated fault gouge. *Journal of Geophysical Research*, *95*(B5), 7007–7025. <https://doi.org/10.1029/JB095iB05p07007>
- Mellier, C., & Kohl, T. (2014). The significance of hydrothermal alteration zones for the mechanical behavior of a geothermal reservoir. *Geothermal Energy*, *2*(1), 12. <https://doi.org/10.1186/s40517-014-0012-2>
- Mitchell, E. K., Fialko, Y., & Brown, K. M. (2016). Velocity-weakening behavior of Westerly granite at temperature up to 600°C. *Journal of Geophysical Research: Solid Earth*, *121*(9), 6932–6946. <https://doi.org/10.1002/2016JB013081>
- Niemeijer, A. R., & Spiers, C. J. (2007). A microphysical model for strong velocity weakening in phyllosilicate-bearing fault gouges. *Journal of Geophysical Research*, *112*(B10). <https://doi.org/10.1029/2007JB005008>
- Nishimoto, S., & Yoshida, H. (2010). Hydrothermal alteration of deep fractured granite: Effects of dissolution and precipitation. *Lithos*, *115*(1–4), 153–162. <https://doi.org/10.1016/j.lithos.2009.11.015>
- Okuda, H., Niemeijer, A. R., Takahashi, M., Yamaguchi, A., & Spiers, C. J. (2023). Hydrothermal friction experiments on simulated basaltic fault gouge and implications for megathrust earthquakes. *Journal of Geophysical Research: Solid Earth*, *128*(1), e2022JB025072. <https://doi.org/10.1029/2022JB025072>
- Paulillo, A., Cotton, L., Law, R., Striolo, A., & Lettieri, P. (2020). Geothermal energy in the UK: The life-cycle environmental impacts of electricity production from the United Downs Deep Geothermal Power project. *Journal of Cleaner Production*, *249*, 119410. <https://doi.org/10.1016/j.jclepro.2019.119410>
- Pirajno, F. (2009). Hydrothermal processes and wall rock alteration. In F. Pirajno (Ed.), *Hydrothermal processes and mineral systems* (pp. 73–164). Springer Netherlands. https://doi.org/10.1007/978-1-4020-8613-7_2
- Psyrillos, A., Burley, S. D., Manning, D. A. C., & Fallick, A. E. (2003). Coupled mineral-fluid evolution of a basin and high: Kaolinization in the SW England granites in relation to the development of the plymouth basin. *Geological Society, London, Special Publications*, *214*(1), 175–195. <https://doi.org/10.1144/gsl.sp.2003.214.01.11>
- Reinecker, J., Gutmanis, J., Foxford, A., Cotton, L., Dalby, C., & Law, R. (2021). Geothermal exploration and reservoir modelling of the United Downs deep geothermal project, Cornwall (UK). *Geothermics*, *97*, 102226. <https://doi.org/10.1016/j.geothermics.2021.102226>
- Ruina, A. (1983). Slip instability and state variable friction laws. *Journal of Geophysical Research*, *88*(B12), 10359–10370. <https://doi.org/10.1029/JB088iB12p10359>
- Savage, D., Cave, M. R., Milodowski, A. E., & George, I. (1987). Hydrothermal alteration of granite by meteoric fluid: An example from the Carnmenellis granite, United Kingdom. *Contributions to Mineralogy and Petrology*, *96*(3), 391–405. <https://doi.org/10.1007/bf00371257>
- Scholz, C. H. (1998). Earthquakes and friction laws. *Nature*, *391*(6662), 37–42. <https://doi.org/10.1038/34097>
- Scholz, C. H. (2019). *The mechanics of earthquakes and faulting* (3 ed.). Cambridge University Press. <https://doi.org/10.1017/9781316681473>
- Scrivener, R. C., Darbyshire, D. P. F., & Shepherd, T. J. (1994). Timing and significance of crosscourse mineralization in SW England. *Journal of the Geological Society*, *151*(4), 587–590. <https://doi.org/10.1144/gsjgs.151.4.0587>
- Shail, R., & Alexander, A. C. (1997). Late carboniferous to triassic reactivation of variscan basement in the western English channel: Evidence from onshore exposures in south Cornwall. *Journal of the Geological Society*, *154*(1), 163–168. <https://doi.org/10.1144/gsjgs.154.1.0163>
- Shail, R., & Simons, B. (2023). The Cornubian Batholith. In *Metallic Resources 1*, S. Decrée (Ed.). <https://doi.org/10.1002/9781394264810.ch2>
- Simons, B., Shail, R. K., & Andersen, J. C. Ø. (2016). The petrogenesis of the Early Permian Variscan granites of the Cornubian Batholith: Lower plate post-collisional peraluminous magmatism in the Rhenohercynian Zone of SW England. *Lithos*, *260*, 76–94. <https://doi.org/10.1016/j.lithos.2016.05.010>
- Skarbak, R. M., & Savage, H. M. (2019). RSFit3000: A MATLAB GUI-based program for determining rate and state frictional parameters from experimental data. *Geosphere*, *15*(5), 1665–1676. <https://doi.org/10.1130/ges02122.1>
- Stefansson, V.-D. (1997). Geothermal reinjection experience. *Geothermics*, *26*(1), 99–139. [https://doi.org/10.1016/S0375-6505\(96\)00035-1](https://doi.org/10.1016/S0375-6505(96)00035-1)
- Summers, R., & Byerlee, J. (1977). A note on the effect of fault gouge composition on the stability of frictional sliding. *International Journal of Rock Mechanics and Mining Sciences & Geomechanics Abstracts*, *14*(3), 155–160. [https://doi.org/10.1016/0148-9062\(77\)90007-9](https://doi.org/10.1016/0148-9062(77)90007-9)
- Takahashi, M., Mizoguchi, K., Kitamura, K., & Masuda, K. (2007). Effects of clay content on the frictional strength and fluid transport property of faults. *Journal of Geophysical Research*, *112*(B8), B08206. <https://doi.org/10.1029/2006JB004678>
- Tembe, S., Lockner, D. A., & Wong, T.-F. (2010). Effect of clay content and mineralogy on frictional sliding behavior of simulated gouges: Binary and ternary mixtures of quartz, illite, and montmorillonite. *Journal of Geophysical Research*, *115*(B3), B03416. <https://doi.org/10.1029/2009jb006383>
- Wang, W., & Scholz, C. H. (1994). Micromechanics of the velocity and normal stress dependence of rock friction. *Pure and Applied Geophysics*, *143*(1–3), 303–315. <https://doi.org/10.1007/BF00874333>
- Yin, T. B., Shu, R. H., Li, X. B., Wang, P., & Liu, X. L. (2016). Comparison of mechanical properties in high temperature and thermal treatment granite. *Transactions of Nonferrous Metals Society of China*, *26*(7), 1926–1937. [https://doi.org/10.1016/S1003-6326\(16\)64311-X](https://doi.org/10.1016/S1003-6326(16)64311-X)
- Zhang, F., Cao, S., An, M., Zhang, C., & Elsworth, D. (2023). Friction and stability of granite faults in the Gonghe geothermal reservoir and implications for injection-induced seismicity. *Geothermics*, *112*, 102730. <https://doi.org/10.1016/j.geothermics.2023.102730>